UV-written silicon nitride integrated optical phased arrays

S. T. Ilie[1], G. De Paoli[1], A. Flint[1], T. Domínguez Bucio[1], P. Ginel-Moreno[2], J. Sagar[3], A. Ortega-Monux[2], K. Lekkas[4], T. Rutirawut[1], L. Mastronardi[1], I. Skandalos[1], I. Molina-Fernandez[2], G.T. Kanellos[4], P. Cheben[5], P. G. R. Smith[1], J. C. Gates[1], F. Y. Gardes[1]

[1] Optoelectronics Research Center, University of Southampton, Southampton SO17 1BJ, UK
[2] Universidad de Malaga, Dpto. de Ingenieria de Comunicaciones, 29071 Malaga, Espana
[3] Quantum Engineering Centre for Doctoral Training, Woodland Road, Bristol, UK
[4] High Performance Networks Group, University of Bristol, Woodland Road, Bristol, UK
[5]National Research Council of Canada, Ottawa, Ontario, K1A 0R6, Canada

ABSTRACT

Silicon nitride (SiNx), has been widely regarded as a CMOS photonics enabling material, facilitating the development of low-cost CMOS compatible waveguides and related photonic components. We have previously developed an NH_3-free SiN PECVD platform in which its optical properties can be tailored. Here, we report on a new type of surface-emitting nitrogen-rich silicon nitride waveguide with antenna lengths of L > 5 mm. This is achieved by using a technique called small spot direct ultraviolet writing, capable of creating periodic refractive index changes ranging from -0.01 to -0.04. With this arrangement, a weak antenna radiation strength can be achieved, resulting in far-field beam widths < 0.015^o, while maintaining a minimum feature size equal to 300 nm, which is compatible with DUV scanner lithography.

Keywords: Optical phased array, UV laser exposure, Silicon Nitride

1. Introduction

Optical phased arrays (OPAs) are believed to be the key to addressing the system requirements of applications such as light detection and ranging (LiDAR) systems for autonomous vehicles or free-space optical communications [1] by enabling precise beam steering and forming capabilities without the need for mechanical or moving components. Previously developed for RF telecommunications purposes, the concept has been enabled on a large scale by the recent developments of silicon photonics, significantly reducing size, weight, and power consumption [2]. Silicon-on-insulator (SOI) is a dominant platform for developing integrated photonic circuits for applications such as biomedical, quantum, sensing and optical interconnects in datacentres. The implementation of high-index contrast waveguides with silicon and silicon dioxide using CMOS-compatible processes allows the fabrication of photonic integrated circuits in large volumes at low cost in silicon photonic foundries. A wide range of SOI devices aimed at optical interconnects including low-loss waveguides, optical filters [3], de-multiplexers [4], modulators [5], photodetectors [6], and integrated lasers [7] have been explored. Nonetheless, the outstanding limitations of Si such as a very large two-photon absorption (TPA) coefficient at telecommunication wavelengths [8], narrow transparency window between 1.1-8 um [9], and high thermo-optic coefficient make devices strongly sensitive to temperature variations. Amongst various alternatives, silicon nitride (SiN_x) has been widely investigated [10], showing promising linear and nonlinear performance. SiN_x exhibits a wide transparency window (250 nm-7 um) [11], low refractive index contrast, negligible TPA, and a low-thermo optic coefficient that is one order of magnitude lower than that of Si [12].

Ongoing research in waveguide-based OPAs has focused on developing coherent system architectures using standard CMOS photonic antennas using multi-etch step gratings [13] and sidewall perturbated waveguide gratings [14]. Due to the high contrast between the waveguide core and the surrounding material, the strength of such antennas results in antenna lengths of up to a few hundred microns before all the light is emitted from the waveguide. Longer antennas, in the order of several millimeters, are required to achieve a narrow far-field radiation pattern for long-range LiDAR applications. To achieve such requirements it is required to fabricate features below 10 nm which are hard to achieve with high precision even with electron-beam lithography

processes. To overcome this problem, a subwavelength segmented core OPA topology has been proposed recently [15,16], enabling precise control of the modal confinement and loading of evanescently coupled radiative elements. Nonetheless, feature sizes as small as 80 nm are still required to fabricate OPAs using this topology. As a result, the use of a silicon nitride waveguide platform has been explored as an alternative solution [17]. Due to its low index contrast compared to the SOI platform, it enables the precise control of the waveguide modulation strength and the fabrication of antennas capable of achieving the same emission strength as their SOI counterparts while using larger feature sizes.

In this manuscript, we propose the use of a technique that has been used to permanently change the behavior of silicon oxide and silicon nitride devices by UV irradiation [18] ($\lambda = 244$ nm) in order to create 1D waveguide integrated antenna structures with radiating elements that are periodically patterned within the waveguide core. We have previously demonstrated [19] the post-fabrication UV laser trimming of nitrogen-rich silicon nitride ring resonators operating in the short-wave infrared spectral region (around 2 um), capable of obtaining a change of -2×10^{-2} in the refractive index of the material while using a laser beam with a spot diameter of 7 um for a few seconds. The induced refractive index change is caused by the structural rearrangement of the bonding configuration of the Si-N bonds and the release of hydrogen [20] from the SiN_x film that is associated with high energy generated by the UV light, causing Si-H and, the N-H bonds to break.

The fabrication flow of the devices starts with 8" Si wafers with a 3 um thermally-grown SiO_2 on top of which a 400 nm SiNx layer (n = 1.9) was deposited at 350 °C using the NH_3-free PECVD process fully detailed in [21]. The devices were then patterned on the wafer using deep ultra-violet (DUV) lithography. After which the exposed features were transferred to the SiNx layer using ICP etching with an etch depth of 400nm. The UV reflective aluminium mask was patterned through windows defined by the second DUV lithography step followed by the sputtering of a 50 nm aluminium layer. The photoresist was lifted-off by sequentially dipping in room temperature acetone and NMP with ultrasonic agitation. After the UV exposure, the aluminium mask was stripped off by dipping in NaOH solution. Finally, a 2 µm SiO_2 top cladding is deposited using PECVD to act as a protective layer.

There are two key advantages of our patterning technique compared to standard CMOS single-etch fabrication methods which allow us to accurately control the grating strength and thus achieve weakly coupled gratings required for long antenna apertures. First, since the waveguide patterns are exposed using a reflective aluminum hard mask, this bypasses the need to etch the patterns to create the antenna, thus removing the high sensitivity to fabrication imperfections such as the vertical sidewall roughness [22] and increasing robustness for a long waveguide grating structure. Second, by using different UV laser fluences and exposure time, we are able to control the induced refractive index change up to -4×10^{-2} resulting in precise control of the grating radiation strength and angle of emission while using the same patterned structures. Furthermore, we are capable of extending the use of such surface-emitting antenna into a waveguide grating array configuration by placing an array of 1D antenna elements uniformly spaced in order to collimate the light in both optical planes xz and yz (Figure 1).

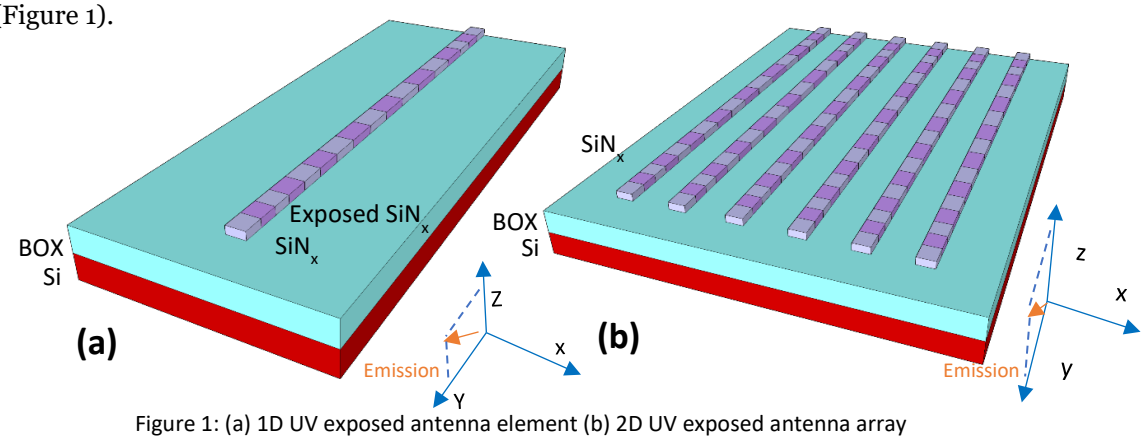

Figure 1: (a) 1D UV exposed antenna element (b) 2D UV exposed antenna array

2. Waveguide grating design

The 1D antenna is designed for a N-rich SiN_x (n = 1.9) platform with a thickness (H) of 400 nm, a 3 um buried oxide (BOX), and a 2 um silicon dioxide (SiO_2) upper cladding. The design parameters for the UV-exposed waveguide grating, i.e., the width (W) and the thickness were chosen to satisfy single mode conditions, but also allow for dual-polarization operation. This antenna grating structure has been designed to operate within the telecom wavelength of 1550 nm using TE polarization. The next step in our antenna design, was to optimize the grating strength (α), which is measured in mm^{-1}. The grating strength and the corresponding antenna length (L), determines the beam width of the diffracted beam in the far-field region. For large apertures (L >> 1 mm), the full width half maximum (FWHM) of the antenna can be approximated to [23]:

$$\Delta\theta = \frac{2\alpha}{k_0 cos(\theta_0)} \quad \textbf{(1)}$$

Where α is the grating modulation strength, $k_o = 2\pi/\lambda_o$ is the wavenumber, λ_o is the wavelength and θ_o is the radiation angle of the antenna in air. The radiation angle is then calculated based on the grating equation [24]:

$$sin(\theta_0) = n_c sin(\theta_c) = n_{eff} - \frac{m\lambda}{\Lambda_g} \quad \textbf{(2)}$$

Where θ_o and θ_c are the diffraction angles in the air and the upper SiO_2 cladding. The n_c is the cladding refractive index, n_{eff} is the effective refractive index of the mode travelling within the waveguide core, m is the diffraction order, λ is the wavelength, and Λ_g is the period of the radiation grating. The far-field region of the grating is characterised in two orthogonal planes: xz and yz (Figure 1). Whereas the beam width θ (in the yz plane) is determined by the length of the antenna, the beam width ϕ (in the yz plane) is related to the far-field radiation pattern of a single antenna or the waveguide spacing between adjacent waveguides in a grating array configuration. In order to quantify the amount of power radiated upwards, we define the radiation efficiency of the antenna, as the ratio between the power radiated upwards and all the power radiated by the antenna (sideways, bottom, and waveguide reflection).

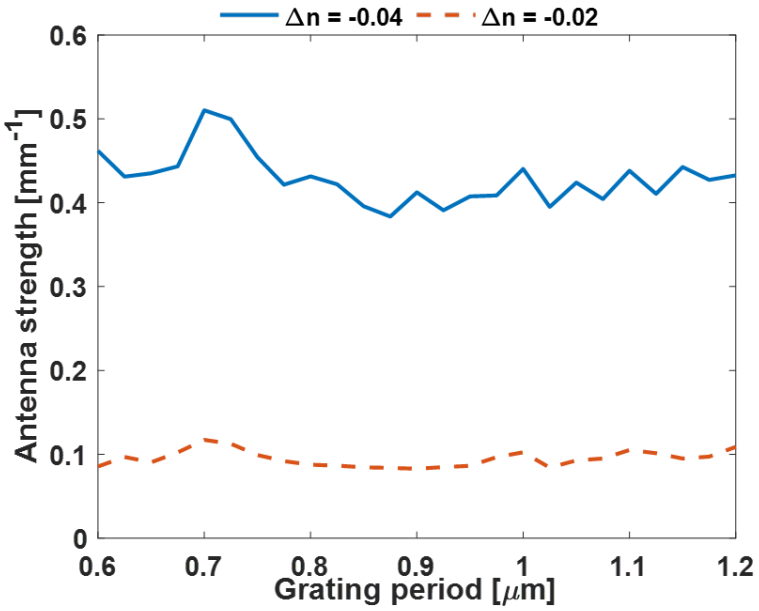

Figure 2: Grating period sweep versus antenna strength of a 1D antenna periodically exposed with a refractive index change of -0.04 and -0.02

To satisfy automotive requirements for LiDAR, a far-field beam width on the order of 0.015° is required. To achieve such a narrow beam width, we calculate from Eq. 1 the corresponding grating strength, in the range of 0.4 – 0.5 mm^{-1}, which results in antenna lengths ranging from 4.6 mm to 5.5 mm. Three-dimensional (3D) finite-difference time-domain (FDTD) simulations of such long antennas would require vast computational resources. As a result, we only simulated a short section comprising 20 um of the periodic grating structure. The calculated antenna perturbation strength is shown in Figure 2 for refractive index changes of -0.02 and -0.04, in which the period of the antenna section is swept between 0.6 and 1.2 um while keeping a fixed DC of 0.5 in order to facilitate DUV lithography dosage testing. The radiation strength obtained from the FDTD simulation was calculated by measuring the power launched into the antenna (P_{in}), the remaining power at the end of the 20 um grating structure, and it was defined as $P_{out} = P_{in} \exp(-2\alpha L)$, resulting in an α = 0.4-0.5 mm^{-1} for grating periods values ranging from 0.6 to 0.825 um.

Figure 3 (a), shows radiation efficiencies ranging from 20% up to 54% when sweeping the period of the antenna section between 0.6 and 1.2 um. Radiation efficiencies exceeding 50% are observed for periods within the 0.75 to 0.85 um range due to constructive interferences created between the BOX and the silicon substrate as a result of the asymmetric structure of the waveguide structure. A drop in the radiation efficiency is observed towards grating periods centred around 1 um (Figure 3 (b)), and we associate these to the normal emission point (Bragg reflection regime), in which the constructive interference between the layers negatively impact the radiation efficiency [25]. Our patterning technique is suitable for obtaining even weaker grating structures using the same waveguide grating period beyond the design target antenna length (>>5 mm), however, we chose to stay within a reasonable margin away from the maximum optical coherence length for a Lorentzian optical spectrum in which a random walk of the optical phase is exhibited.

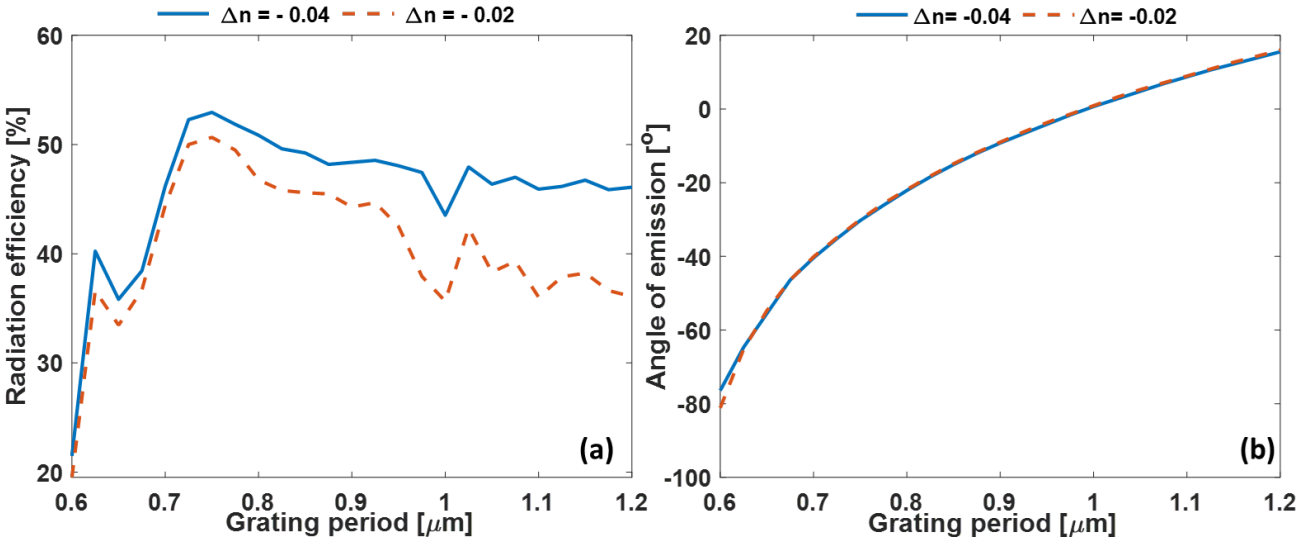

Figure 3: Grating period sweep versus radiation efficiency (a) and angle of emission (b) of a 1D antenna periodically exposed with a refractive index change of -0.04 and -0.02

The tuning range of the antenna against 200 nm wavelength span while using a fixed grating period of 800 nm for periodic refractive index changes of -0.04 and -0.02 is presented in Figure 4. When considering the dispersive nature of the grating couplers, one would steer the beam in the orthogonal direction by changing the input laser wavelength. By performing a linear of the emission angles of the antenna as a function of the wavelength, we calculate a wavelength sensitivity of -0.09007 °/nm and respectively -0.09046 °/nm for a refractive index change of -0.04 and -0.02. For a period of 800 nm and a periodic refractive index change of -0.04, the corresponding antenna strength is α = 0.423 mm^{-1}, achieving a radiation efficiency of 51.3%. This

results in an equivalent L = 5.44 mm to radiate 99% of the input power. Using Eq. 1, this grating length yields a corresponding far-field beam width of 0.0128°, radiating at $\theta_o = -22^o$.

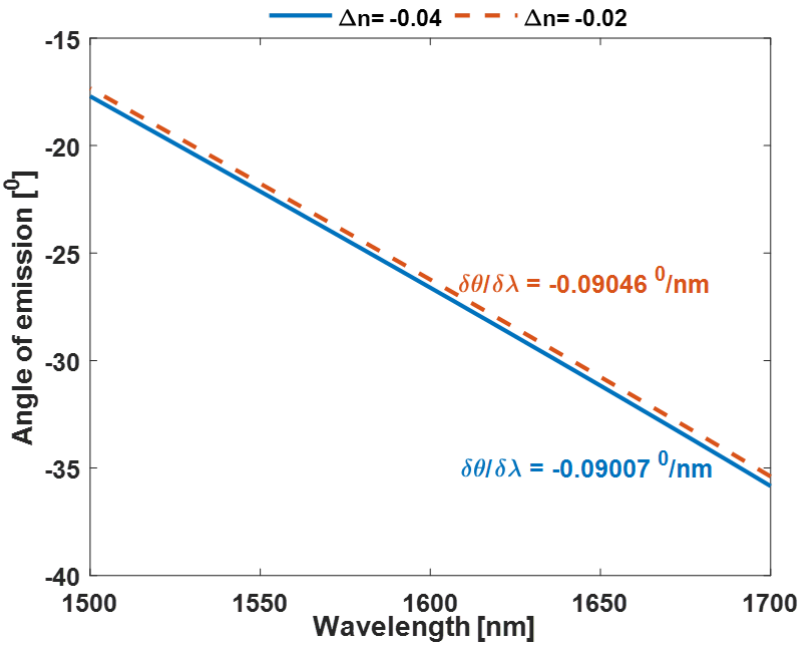

Figure 4: Wavelength sensitivity of the 1D antenna periodically exposed with a refractive index change of -0.04 and -0.02

While using the single element antenna configuration, the far-field beam width $(\lambda/\pi w)$ in the xz plane (Figure 1) is estimated to be equal to $\Delta\phi = 28^o$, where w is the antenna lateral width. In order to reduce the beam width within the ϕ-direction, we propose a waveguide grating array design able to achieve 2D beam steering and collimation. This is achieved by adjusting the phase profile within each of the radiation elements and by tuning the wavelength in the other direction. We use Lumerical MODE solutions to estimate the minimum distance between adjacent waveguides by calculating the difference in the symmetric and anti-symmetric hybrid nodes (Δneff) and then calculate the length required to couple 10% power within a 5 mm long waveguide for various waveguide geometries, resulting in an ideal waveguide spacing of 3.25 um. The refractive indices of SiO_2 and N-rich SiN_x used in the simulations have been determined by ellipsometry. One can estimate the field of view (FOV) of the 2D waveguide-grating array as:

$$|\theta_x| < 2\sin^{-1}\frac{\lambda}{2d} \quad \textbf{(3)}$$

Where θ_x is the FOV, λ is the wavelength in free space and d is the waveguide spacing between two adjacent waveguides, resulting in a FOV of 27.6° in this waveguide array configuration. A 3D simulated far field pattern, assuming a gaussian decaying spectrum of the amplitudes in each of the waveguides within the grating array which consists of 32 antennas that are 20 um long, emitting at θ = -22° and φ = 0° is presented within Figure 5, showing a FOV of 29.1°, which closely matches the analytical estimations of a diffraction-limited OPA.

The reported results, summarized in Table 1, are unique for a single-etch step SiN_x-based antenna with a minimum feature size of 300 nm, in contrast with state-of-the-art Si and SiN_x antenna designs that require small feature sizes below 100 nm or complex fabrication processes to obtain comparable grating modulation strengths. Thus, this manuscript demonstrates that weak large-scale antennas can be realized in the SiN_x platform while maintaining compatibility with modern deep-UV lithography technology platforms.

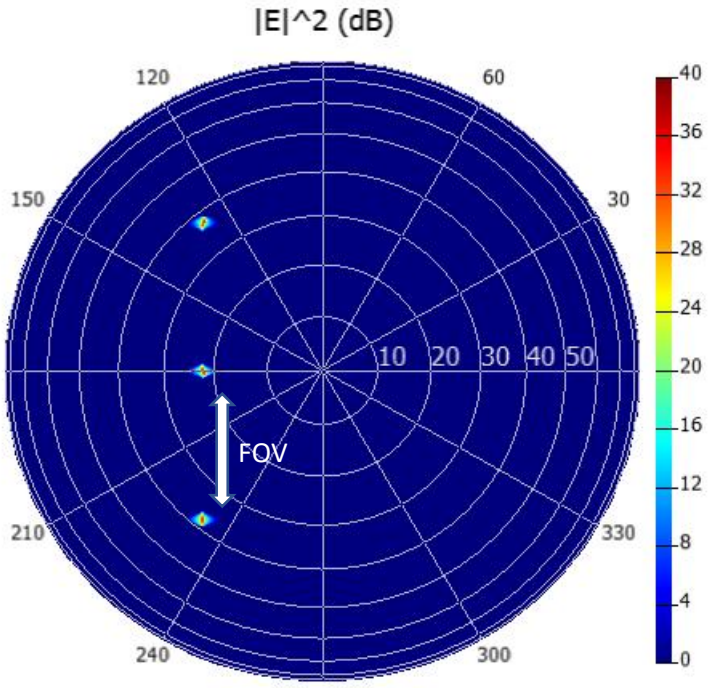

Figure 5: 3D FDTD far-field estimation in polar coordinates of a 2D OPA topology consisting of an 32-element antenna array uniformly spaced at 3.25 um

Table 1: State-of-the-art SOI and SiN_x 1D OPAs

Material platform	Grating design	Feature size [nm]	Beam width[^{0}]	Reference
SiN	UV exposure	300	0.015	This work
SOI	Full-etch WGA	7	0.15	[26]
SOI	Subwavelength	80	0.025	[15]
SiN	Multi-etch step	500	0.2	[27]
SiN	Full-etch WGA	70	0.02	[17]
SiN-Si	Dual-layer WGA	390	0.47	[28]

3. Conclusion

To summarize, we have implemented a 1D single-element antenna element in an N-rich SiN platform, in which the antenna radiation strength can be efficiently controlled by post-fabrication UV laser exposure capable of refractive index changes within the N-rich SiN thin film ranging from -0.01 to -0.04. This allowed us to achieve a length of 5.44 mm for SiN-based antennas with a corresponding FWHM of 0.0128^o and a radiation efficiency of 51.3%. Furthermore, we have also demonstrated the implementation of such a single-element antenna within a larger waveguide grating array topology, capable of achieving a FOV of 29.1^o when using a 32-element array in the ϕ-direction.

ACKNOWLEDGEMENTS

The authors acknowledge the support of the Engineering and Physical Sciences Research Council (EPSRC) (EP/R003076/1, EP/R513325/1, EP/N013247/1) and H2020 ICT-PLASMONIAC.

REFERENCES

[1] Streshinsky, M., et al. "The road to affordable, large-scale silicon photonics." Optics and Photonics News 24.9 (2013): 32-39.
[2] Van Acoleyen, Karel, et al. "Off-chip beam steering with a one-dimensional optical phased array on silicon-on-insulator." Optics letters 34.9 (2009): 1477-1479.
[3] Jalali, Bahram, and Sasan Fathpour. "Silicon photonics." Journal of lightwave technology 24.12 (2006): 4600-4615.
[4] Won, Rachel. "Integrating silicon photonics." Nature photonics 4.8 (2010): 498-499.
[5] Reed, Graham T., et al. "Silicon optical modulators." Nature photonics 4.8 (2010): 518-526.
[6] Ahn, Donghwan, et al. "High performance, waveguide integrated Ge photodetectors." Optics express 15.7 (2007): 3916-3921.
[7] Rong, Haisheng, et al. "An all-silicon Raman laser." Nature 433.7023 (2005): 292-294.
[8] Bristow, Alan D., Nir Rotenberg, and Henry M. Van Driel. "Two-photon absorption and Kerr coefficients of silicon for 850–2200 nm." Applied Physics Letters 90.19 (2007): 191104.
[9] Miller, Steven A., et al. "Low-loss silicon platform for broadband mid-infrared photonics." Optica 4.7 (2017): 707-712.
[10] Muñoz, Pascual, et al. "Silicon nitride photonic integration platforms for visible, near-infrared and mid-infrared applications." Sensors 17.9 (2017): 2088.
[11] Rahim, Abdul, et al. "Expanding the silicon photonics portfolio with silicon nitride photonic integrated circuits." Journal of lightwave technology 35.4 (2017): 639-649.
[12] Bucio, Thalía Domínguez, et al. "Silicon nitride photonics for the near-infrared." IEEE Journal of Selected Topics in Quantum Electronics 26.2 (2019): 1-13.
[13] Sun, Jie, et al. "Large-scale nanophotonic phased array." Nature 493.7431 (2013): 195-199.
[14] Poulton, Christopher V., et al. "Coherent solid-state LIDAR with silicon photonic optical phased arrays." Optics letters 42.20 (2017): 4091-4094.
[15] Ginel-Moreno, Pablo, et al. "Highly efficient optical antenna with small beam divergence in silicon waveguides." Optics Letters 45.20 (2020): 5668-5671.
[16] Ginel-Moreno, Pablo, et al. "Millimeter-long metamaterial surface-emitting antenna in the silicon photonics platform." Optics Letters 46.15 (2021): 3733-3736.
[17] Poulton, Christopher V., et al. "Large-scale silicon nitride nanophotonic phased arrays at infrared and visible wavelengths." Optics letters 42.1 (2017): 21-24.
[18] Haeiwa, Hirofumi, Toshiki Naganawa, and Yasuo Kokubun. "Wide range center wavelength trimming of vertically coupled microring resonator filter by direct UV irradiation to SiN ring core." IEEE Photonics Technology Letters 16.1 (2004): 135-137.
[19] De Paoli, Greta, et al. "Laser trimming of the operating wavelength of silicon nitride racetrack resonators." Photonics Research 8.5 (2020): 677-683.
[20] Charifi, Hicham, et al. "Opto-structural properties of silicon nitride thin films deposited by ECR-PECVD." World Journal of Condensed Matter Physics 6.01 (2016): 7.
[21] Bucio, Thalía Domínguez, et al. "Material and optical properties of low-temperature NH3-free PECVD SiNx layers for photonic applications." Journal of Physics D: Applied Physics 50.2 (2016): 025106.
[22] M. C. M. Lee and M. C. Wu, “Thermal annealing in Hydrogen for 3-D profile transformation on silicon-oninsulator and sidewall roughness reduction,” Journal of Microelectromechanical Systems, vol. 15, no. 2, pp. 338–343, 2006
[23] Fuscaldo, Walter, David R. Jackson, and Alessandro Galli. "Beamwidth properties of endfire 1-D leaky-wave antennas." IEEE Transactions on Antennas and Propagation 65.11 (2017): 6120-6125.
[24] Halir, Robert, et al. "Waveguide sub-wavelength structures: a review of principles and applications." Laser & Photonics Reviews 9.1 (2015): 25-49.

[25] Cheben, Pavel, et al. "Subwavelength integrated photonics." Nature 560.7720 (2018): 565-572.
[26] Kim, Taehwan, et al. "A single-chip optical phased array in a wafer-scale silicon photonics/CMOS 3D-integration platform." *IEEE Journal of Solid-State Circuits* 54.11 (2019): 3061-3074.
[27] Im, Chul-Soon, et al. "Silicon nitride optical phased array based on a grating antenna enabling wavelength-tuned beam steering." Optics express 28.3 (2020): 3270-3279.
[28] Dwivedi, S., et al. "Calibration-free Si-SiN optical phased array." Integrated Photonics Research, Silicon and Nanophotonics. Optical Society of America, 2019.